

THE TEMPERATURE OF HOT GAS HALOS OF EARLY-TYPE GALAXIES

S. PELLEGRINI

Astronomy Department, University of Bologna, via Ranzani 1, 40127 Bologna, Italy
email: silvia.pellegrini@unibo.it

ABSTRACT

Recently, the temperature T and luminosity L_X of the hot gas halos of early type galaxies have been derived with unprecedented accuracy from *Chandra* data, for a sample of 30 galaxies covering a wider range of galactic luminosity (and central velocity dispersion σ_c) than before. This work investigates the origin of the observed temperatures, by examining the relationship between them and the galaxy structure, the gas heating due to Type Ia supernovae (SNIa's) and the gravitational potential, and the dynamical status of the gas flow. In galaxies with $\sigma_c \lesssim 200 \text{ km s}^{-1}$, the T 's are close to a fiducial average temperature for the gas when in outflow; at $200 < \sigma_c (\text{km s}^{-1}) < 250$, the T 's are generally lower than this, and unrelated with σ_c , which requires a more complex gas flow status; at larger σ_c , the T 's may increase as σ_c^2 , as expected for infall heating, though heating from SNIa's, independent of σ_c , should be dominant. All observed T 's are larger than the virial temperature, by up to $\sim 0.5 \text{ keV}$. This additional heating can be provided in the X-ray brightest galaxies by SNIa's and infall heating, with a SNIa's energy input even lower than in standard assumptions; in the X-ray fainter ones it can be provided by SNIa's, whose energy input would be required close to the full standard value at the largest σ_c . This same energy input, though, would produce temperatures larger than observed at low σ_c , if entirely thermalized. The values of the observed T 's increase from outflows to inflows; the gas is relatively hotter in outflows, though, if the T 's are rescaled by the virial temperature. For $200 < \sigma_c (\text{km s}^{-1}) < 250$, lower L_X values tend to correspond to lower T 's, which deserves further investigation.

Subject headings: galaxies: elliptical and lenticular, CD — galaxies: fundamental parameters — galaxies: ISM — galaxies: kinematics and dynamics — X-rays: galaxies — X-rays: ISM

1. INTRODUCTION

The advent of the *Chandra* X-ray observatory, with its unprecedented sub-arcsecond resolution, allowed to study better than ever before the main contributors to the total X-ray emission of early-type galaxies (hereafter ETGs): the low-mass X-ray binaries (LMXBs; Fabbiano 2006), a population of weak sources as late type stellar coronae, cataclismic variables, and coronally active binaries (Pellegrini & Fabbiano 1994, Revnivtsev et al. 2008), the nuclear emission due to a supermassive black hole (MBH; e.g., Gallo et al. 2010, Pellegrini 2010), and a hot interstellar medium (ISM) with a temperature of a few million degrees. After careful subtraction of the stellar (resolved and unresolved) and nuclear emissions, the properties of the hot ISM could be characterized with unprecedented accuracy. Recently, this has been done for a sample of 30 normal (non-cD) ETGs observed with *Chandra* to a depth ensuring the detection of bright LMXBs (Borson et al. 2011, hereafter BKF). This is the first X-ray sample of ETGs covering a wide range of galactic luminosity, central velocity dispersion σ_c , and hot gas emission L_X , and with the X-ray properties of the hot gas (e.g., luminosity L_X and average temperature T) derived in a homogeneous way, using a complete and accurate procedure to subtract all kinds of non-gaseous emission (nucleus, detected and undetected LMXBs, and unresolved weak stellar sources). This approach resulted in a larger fraction of hot gas-poor galaxies than in previous samples, with L_X extending down to much lower values than before ($\sim 10^{38} \text{ erg s}^{-1}$), and showing a varia-

tion of up to ~ 3 orders of magnitude at the same galactic luminosity (see also David et al. 2006, Diehl & Statler 2007, Memola et al. 2009). Such a wide variation, even larger than previously found, had been linked to the origin and evolution of the hot ISM, and had provided evidence for the effectiveness of an internal heating mechanism (as from type Ia supernovae, hereafter SNIa's) to regulate the gas evolution and produce its very different content in ETGs at the present epoch (Loewenstein & Mathews 1987, David et al. 1990, Ciotti et al. 1991); the action of external agents (gas stripping, confinement, accretion) to reduce or enhance the gas content was also invoked (e.g., White & Sarazin 1991, Brown & Bregman 2000, Sun et al. 2007).

With this new characterization of the hot gas, BKF revisited the relationships between fundamental properties of the hot gas and of the host galaxy, as the $L_X - T$, $L_X - \sigma_c$ and $T - \sigma_c$ relations, where σ_c is a representative measure of the depth of the galactic potential well (Eskridge et al. 1995, O'Sullivan et al. 2001, 2003). L_X correlates positively with T and σ_c , though with a wide variation at fixed σ_c and T . Interestingly, the best fit relation $L_X \propto T^{4.5}$, close to what already known for X-ray luminous ETGs (O'Sullivan et al. 2003), is still moderately strong among ETGs with low T and L_X ; also, in the $L_X - \sigma_c$ relation, ETGs with $kT > 0.4 \text{ keV}$ are the X-ray brightest (with one exception), while those with $kT < 0.3 \text{ keV}$ are the X-ray faintest. The least gas rich ETGs are then the coolest ones, which seemed contrary to expectation, if low L_X ETGs loose their ISM in an outflow (e.g.,

David et al. 1990, Ciotti et al. 1991), and the hotter the gas, the stronger is the outflow (BKF). On average T increases with σ_c , and most ETGs lie above a rough estimate of the gas virial temperature ($T_\sigma = \mu m_p \sigma_c^2 / k$), suggesting the presence of additional heating. ETGs with a moderate to high gas content ($L_X > 5 \times 10^{39} \text{ erg s}^{-1}$) follow a trend roughly parallel to that of T_σ ; instead, ETGs with little hot gas ($L_X < 5 \times 10^{39} \text{ erg s}^{-1}$) have a similar temperature for σ_c ranging from 160 to 250 km s^{-1} . This lack of correlation was attributed to a different dynamical state of the hot ISM in gas-poor with respect to gas-rich ETGs, though a full explanation of this aspect remained to be found (BKF).

This work takes advantage of the new accurate measurements of the hot gas properties, and of the fundamental relations $L_X - \sigma_c$ and $T - \sigma_c$, derived down to galaxy masses and X-ray luminosities smaller than ever before (BKF), to investigate the relationship between T , the galaxy structure, the internal gas heating mechanisms (SNIa's, and those linked to the gravitational potential), and the dynamical status of the gas flow. To this purpose, a few characteristic temperatures are introduced, depending on the nature of the gas heating sources and the galaxy structure, and relevant for the various gas flow phases; these characteristic temperatures are then compared with the observed T values. In doing so, galaxy mass models are built according to the most recent understanding of the ETGs' structure, such as their stellar mass profile and their dark matter content and distribution, as indicated by detailed modeling of optical observations and by the main scaling laws (e.g., Cappellari et al. 2006, Weijmans et al. 2009, Auger et al. 2010, Napolitano et al. 2010, Shen & Gebhardt 2010). The aims are to address the following questions: can the gas heating sources above account for the observed T 's? how are the various input energy sources for the gas used in the different flow phases? is there any relation between T and the flow phase?

We present in Sect. 2 the sources of mass and heating for the hot ISM, in Sect. 3 the conditions for the gas to escape from the galaxy, in Sect. 4 the galaxy mass models, in Sect. 5 the comparison between observed and predicted temperatures, in Sect. 6 the relation between gas temperature and flow status, and in Sect. 7 the conclusions.

2. SOURCES OF MASS AND HEATING FOR THE HOT GAS

2.1. Gas Mass

In ETGs the hot gas comes from stellar mass losses produced by evolved stars, mainly during the red giant, asymptotic giant branch, and planetary nebula phases, and by SNIa's, that are the only ones observed in an old stellar population (e.g., Cappellari et al. 1999). The first, more quiescent, type of losses originates ejecta that initially have the velocity of the parent star, then individually interact with the mass lost from other stars or with the hot ISM, and mix with it (Mathews 1990, Parriott & Bregman 2008).

For a galaxy of total stellar mass M_* , the evolution of the stellar mass loss rate $\dot{M}_*(t)$ can be calculated using single burst stellar population synthesis models (Maraston 2005), for a Salpeter and for a Kroupa Initial Mass Function (IMF), assuming for example solar abundance.

So doing, at an age of 12 Gyrs, a rate is recovered of $\dot{M}_* = B \times 10^{-11} L_B(L_{B,\odot}) M_\odot \text{yr}^{-1}$, where L_B is the galactic B-band luminosity at an age of 12 Gyr, and $B=1.8$ or $B=1.9$ for the Salpeter or Kroupa IMF (see also Pellegrini 2011). This value is in reasonable agreement with the average derived for nine local ETGs from *ISO* data (Athey et al. 2002) of $\dot{M}_* = 7.8 \times 10^{-12} L_B(L_{B,\odot}) M_\odot \text{yr}^{-1}$, an estimate based on individual observed values that vary by a factor of ~ 10 , though, which was attributed to different ages and metallicities.

The total mass loss rate of a stellar population \dot{M} is given by the sum $\dot{M} = \dot{M}_* + \dot{M}_{\text{SN}}$, where \dot{M}_{SN} is the rate of mass loss via SNIa events for the whole galaxy. \dot{M}_{SN} is given by $\dot{M}_{\text{SN}} = M_{\text{SN}} R_{\text{SN}}$, where $M_{\text{SN}} = 1.4 M_\odot$ is the ejected mass by one event, and R_{SN} is the explosion rate. R_{SN} has been determined for local ETGs to be $R_{\text{SN}} = 0.16 (H_0/70)^2 \times 10^{-12} L_B(L_{B,\odot}) \text{yr}^{-1}$, where H_0 is the Hubble constant in units of $\text{km s}^{-1} \text{Mpc}^{-1}$ (Cappellari et al. 1999). More recent measurements of the observed rates of supernovae in the local Universe (Li et al. 2010) give a SNIa's rate in ETGs consistent with that of Cappellari et al. (1999). For $H_0 = 70 \text{ km s}^{-1} \text{Mpc}^{-1}$, one obtains $\dot{M}_{\text{SN}} = 2.2 \times 10^{-13} L_B(L_{B,\odot}) M_\odot \text{yr}^{-1}$, that is ~ 80 times smaller than \dot{M}_* derived above for an age of 12 Gyr; therefore, the main source of mass for the hot gas is provided by \dot{M}_* . A reasonable assumption is that the gas is shed by stars with a radial dependence that follows that of the stellar distribution, so that the density profile of the injected gas is $\rho_{\text{gas}}(r) \propto \rho_*(r)$, where $\rho_*(r)$ is the stellar density profile. This assumption is adopted hereafter, and the characteristic temperatures presented below apply to a gas distribution following $\rho_{\text{gas}}(r) \propto \rho_*(r)$ (but see also Sect. 5).

2.2. Heating from stellar motions and supernovae

The material lost by stars is ejected at a velocity of few tens of km s^{-1} and at a temperature of $\lesssim 10^4 \text{ K}$ (Parriott & Bregman 2008), and is subsequently heated to high, X-ray emitting temperatures by the thermalization of the stellar velocity dispersion, as it collides with the mass lost from other stars, or with the ambient hot gas, and is shocked. Another source of heating for the stellar mass losses is provided by the thermalization of the kinetic energy of SNIa's events. The internal energy given by these heating processes to the unit mass of injected gas is $3kT_{inj}/2\mu m_p$ (with k the Boltzmann constant, m_p the proton mass, μm_p the mean particle mass, with $\mu = 0.62$ for solar abundance); T_{inj} is determined by the heating due to thermalization of the motions of the gas-losing stars (T_{star}), and of the velocity of the SNIa's ejecta (T_{SN}), and is written as (e.g., Gisler 1976, White & Chevalier 1983):

$$T_{inj} = T_{star} + T_{SN} = \frac{\dot{M}_* T_* + \dot{M}_{\text{SN}} T_{ej}}{\dot{M}}. \quad (1)$$

Here T_* is the equivalent temperature of the stellar motions (see below), and $T_{ej} = 2\mu m_p E_{\text{SN}} / (3k M_{\text{SN}})$ is the equivalent temperature of the kinetic energy E_{SN} of the SNIa's ejecta, with $E_{\text{SN}} = 10^{51} \text{ erg}$ for one event (e.g., Larson 1974). T_{ej} can be calculated assuming that a factor f of E_{SN} is turned into heat; $f < 1$, since radiative energy losses from expanding supernova remnants

may be important, and values down to $f = 0.1$ have been adopted (Larson 1974, Chevalier 1974); a value of $f = 0.85$ could be not too far off for the hot diluted ISM of ETGs (e.g., Tang & Wang 2005). In this way, $T_{ej} = (f/0.85)1.5 \times 10^9 \text{K}$. From approximating $\dot{M} \simeq \dot{M}_*$, and using the estimates of Sect. 2.1 for \dot{M}_{SN} and \dot{M}_* (for a Kroupa IMF) at the present epoch, one obtains $T_{SN} \simeq 1.7(f/0.85) \times 10^7 \text{K}$.

The injection temperature T_{inj} is then the sum of two parts: one (T_{SN}) is independent of the position within the galaxy where the gas is injected (e.g., independent of radius in spherical symmetry), and is also constant from galaxy to galaxy (for fixed IMF and age of the stellar population, and SNIa's rate); for each ETG it can, though, evolve with time, if \dot{M}_{SN} and \dot{M}_* evolve differently with time (Ciotti et al. 1991). The other part (T_{star}) is instead basically independent of time, but has a radial dependence, and changes with the galaxy structure, i.e., with the total mass and its distribution. An average T_* is obtained calculating the gas mass-weighted temperature gained by the thermalization of the stellar random motions, $\langle T_* \rangle$:

$$\langle T_* \rangle = \frac{1}{k} \frac{\mu m_p}{M_*} \int 4\pi r^2 \rho_*(r) \sigma^2(r) dr, \quad (2)$$

where $\sigma(r)$ is the one-dimensional velocity dispersion of the stars. The integral term in Eq. 2 is the same that gives the kinetic energy associated with the stellar random motions [$E_{kin} = 1.5 \int 4\pi r^2 \rho_*(r) \sigma^2(r) dr$], and that enters the virial theorem for the stellar component; the mass-weighted temperature in Eq. 2 is then often called “gas virial temperature”. For a galaxy mass model made of stars and dark matter, characterized by $\mathcal{R} = M_h/M_*$, where M_h is the total dark mass, and $\beta = r_h/r_*$, with r_h and r_* the scale radii of the two mass distributions, $\langle T_* \rangle$ can be expressed using the central velocity dispersion σ_c as $\langle T_* \rangle = \mu m_p \sigma_c^2 \Omega(\mathcal{R}, \beta)/k$ (e.g., Ciotti & Pellegrini 1992). The function Ω increases mildly for larger \mathcal{R} and for lower β , that is for a larger amount of gravitating mass or a higher mass concentration, but always $\Omega < 1$, since $\sigma(r)$ has in general a negative radial gradient (e.g., Sect. 4 and Fig. 1 below). $\langle T_* \rangle$ is then proportional to σ_c^2 , and a simplified version of the virial temperature in Eq. 2 that is often used is $T_\sigma = \mu m_p \sigma_c^2/k$; T_σ of course overestimates the true $\langle T_* \rangle$.

The mass-averaged injection temperature is finally given by

$$\langle T_{inj} \rangle = \langle T_* \rangle + 1.7(f/0.85) \times 10^7 \text{K}, \quad (3)$$

where in general the second term dominates, as is shown in Sect. 5 below.

2.3. Heating during Infall

In case of mass losses flowing to the galactic center, the gas can be heated due to infall in the galactic potential and adiabatic compression; this process is sometimes referred to as “gravitational heating”. The average change in gravitational energy per unit gas mass inflowing through the galactic potential down to the galactic center is

$$E_{grav}^+ = \frac{1}{M_*} \int_0^\infty 4\pi r^2 \rho_*(r) [\phi(r) - \phi(0)] dr, \quad (4)$$

for galaxy mass distributions with a finite value of $\phi(0)$ (see also Ciotti et al. 1991). One can define a temperature equivalent to the energy in Eq. 4 as $\langle T_{grav}^+ \rangle = 2\mu m_p E_{grav}^+/3k$. As $\langle T_* \rangle$, also $\langle T_{grav}^+ \rangle$ is $\propto \sigma_c^2$, and increases for larger \mathcal{R} and smaller β , which, for inflowing gas, can be understood as a larger gas heating by compression during infall for a larger dark matter amount or its higher concentration.

Not all of E_{grav}^+ can be available for heating, though. If the inflow keeps quasi-hydrostatic, then, by the virial theorem, the energy radiated away is roughly one-half of the change in the gravitational potential energy, and that available for the heating of the gas is the remaining half¹ (i.e., $\sim 0.5E_{grav}^+$). Actually, the energy available for heating will be much less than this. Inflows are caused by the radiative losses produced by the accumulation of the stellar mass return, that makes the cooling time lower than the galactic age; in the central regions, within a radius of ~ 1 kpc, the cooling time can be as short as $\lesssim 10^8$ yr, even shorter than the infall time (e.g., Sarazin & White 1988, Pellegrini 2011). In these conditions, the gas departs from a slow inflow, becomes very dense and supersonic close to the center, and cools rapidly down to low temperatures, so that $> 0.5E_{grav}^+$ is radiated away or goes into kinetic energy of condensations (Sarazin & Ashe 1989). Furthermore, there is the possibility that not all the gas reaches hot the galactic central region, if thermal instabilities develop and produce drop-outs from the flow; if gas cools and condenses out of the flow at large radii, then E_{grav}^+ can be much lower than in the definition above, and heating due to infall in the gravitational potential is “lost” (Sarazin & Ashe 1989). In conclusion, without a precise knowledge of how to compute E_{grav}^+ (which depends on the radius at which the injected gas drops below X-ray emitting temperatures), and about what fraction of E_{grav}^+ is radiated or goes into kinetic energy of the condensations, $\langle T_{grav}^+ \rangle$ remains a reference value; a more direct use can instead be made of the analogous temperature for escape $\langle T_{grav}^- \rangle$ introduced in Sect. 3 below.

2.4. Heating from a central MBH

Due to the presence of a central MBH in ETGs, another potential source of heating for the gas could be provided by nuclear accretion. This subject has been studied intensely recently, through both observations and modeling, and it appears that the energy provided by accretion is of the order of that needed to offset cyclically the cooling of the inflowing gas in the central regions of gas-rich ETGs (e.g., Bîrzan et al. 2004, Million et al. 2010). Therefore, the central MBH is believed to be a heat source that balances the radiative losses of the gas, acting mostly in the central cooling region. In gas poor ETGs the nuclear accretion energy is far lower due to the very small mass accretion rate, if present (Pellegrini et al. 2007), and the absorption of the energy output from accretion is likely not efficient. Given the role of the MBH outlined above, possible energy input from the

¹ The energy lost in radiation and that converted into heat are actually each equal to $0.5E_{grav}^+$ for a self-gravitating gas; for gas in an external potential, the result should remain roughly valid (Binney & Tremaine 1987).

MBH will not be considered as a source of global heating for the gas.

3. CONDITIONS FOR ESCAPE

Another characteristic temperature for comparison with observed T values is the temperature with which the gas can escape from the galaxy. Assuming that the flow is stationary and adiabatic, the Bernoulli constant on each streamline along which the gas flows out of the galaxy must be positive. The Bernoulli equation with the minimum energy for escape is written as $H(r) + v^2(r)/2 + \phi(r) = 0$, where $H = \frac{\gamma}{\gamma-1} \frac{kT}{\mu m_p} = \frac{c_s^2}{\gamma-1}$ is the enthalpy per unit gas mass, γ is the ratio of specific heats, c_s is the sound velocity, and v is the flow velocity. Integrating over the galaxy volume and gas-mass averaging, this condition becomes:

$$\int_0^\infty 4\pi r^2 \rho_*(r) H(r) dr + \frac{1}{2} \int_0^\infty 4\pi r^2 \rho_*(r) v^2(r) dr = M_* E_{\text{grav}}^- \quad (5)$$

where the escape energy

$$E_{\text{grav}}^- = -\frac{1}{M_*} \int_0^\infty 4\pi r^2 \rho_*(r) \phi(r) dr \quad (6)$$

is the average energy required to remove from the galaxy the unit gas mass. E_{grav}^- gives a minimum energy requirement, since energy losses due to cooling may be present; but these are not important for outflows that typically have a low density (e.g., Sect. 5.3 below). The escape temperature equivalent to E_{grav}^- is $\langle T_{\text{grav}}^- \rangle = 2\mu m_p E_{\text{grav}}^- / 3k$. The condition for the minimum energy for escape can then be translated into a condition for the injection temperature of the gas $\langle T_{inj} \rangle$ to be larger than $\langle T_{\text{grav}}^- \rangle$. In the simple case that $\phi(r)$ is due only to one (stellar) mass component, from $\langle T_* \rangle = 2\mu m_p E_{kin} / 3k M_*$ and the virial theorem (Sect. 2), one derives that $\langle T_{\text{grav}}^- \rangle = 4 \langle T_* \rangle$. The estimates of E_{grav}^- in Eq. 6 and then of $\langle T_{\text{grav}}^- \rangle$ will be calculated below for a general mass model (e.g., made by the superposition of stars and dark matter, with a different radial distribution). In previous works, the sufficient condition for the existence of a galactic wind was that the injection temperature exceeded an “escape temperature”, defined as $2T_\sigma$ (White & Chevalier 1983), or “twice the equivalent dark halo temperature” (Loewenstein & Mathews 1987), coupled with the request for the radiative cooling time in the central part of the galaxy to be longer than the time required to flow out of this region. These conditions are similar to imposing that $\langle T_{inj} \rangle$ exceeds $\langle T_{\text{grav}}^- \rangle$ as derived above.

In principle the gas can escape with different combinations of v and T , and the observed T should be close² to that entering H in Eq. 5. There are two extreme cases for the value of the flow velocity v with respect to c_s (i.e., to the temperature). One is when the material is brought to infinity keeping a subsonic velocity, then the minimum

energy requirement becomes $H \approx -\phi$; neglecting the kinetic term in Eq. 5, one then obtains a characteristic gas-mass averaged subsonic escape temperature:

$$\langle T_{\text{esc}}^{sub} \rangle = \frac{2\mu m_p}{5kM_*} \int_0^\infty 4\pi r^2 \rho_*(r) \phi(r) dr = \frac{3}{5} \langle T_{\text{grav}}^- \rangle. \quad (7)$$

In a general case, $H \approx -\phi$ gives for T a larger requirement than obtained when v is not neglected; also the partition of the gas energy between enthalpy and kinetic energy can vary with radius within a galaxy. All this means that $\langle T_{\text{esc}}^{sub} \rangle$ represents a fiducial upper limit to the observed temperatures of outflowing gas: if the kinetic energy of the flow is important, then the actual gas temperature will be lower (the stronger the outflow, with respect to c_s , the cooler the gas). At the opposite extreme case where the “temperature” contribution to the gas energy is minor and that of the velocity is dominant, the Bernoulli equation reduces to $v_{\text{esc}}^2/2 + \phi = 0$; this gives the usual escape velocity of a unit mass from a potential well: $v_{\text{esc}}(r) = \sqrt{2|\phi(r)|}$.

Finally, $\langle T_{\text{grav}}^- \rangle$ and $\langle T_{\text{esc}}^{sub} \rangle$ have the same dependence as $\langle T_* \rangle$ on σ_c^2 , \mathcal{R} , β . For the representative galaxy mass models used here (Sect. 4, Fig. 2), $E_{\text{grav}}^- = (1.7 - 2.3) E_{\text{grav}}^+$; since $\lesssim 0.5 E_{\text{grav}}^+$ can be converted into heat, then the corresponding temperature gained by infall will be $T_{infall} \lesssim \langle T_{\text{grav}}^- \rangle$.

4. GALAXY MASS MODELS

In this work the exact values of $\langle T_* \rangle$, $\langle T_{\text{esc}}^{sub} \rangle$ and $\langle T_{\text{grav}}^- \rangle$ are calculated as a function of σ_c , for a series of representative 3-component galaxy mass models, made by the superposition of a stellar distribution and a dark matter halo, to which a central MBH is added. The stellar density profile is given by the deprojection of a Sérsic law with index $n = 4$ or 5 , as appropriate for ETGs of the luminosities considered in this work (e.g., Kormendy et al. 2009). The mass of the MBH is $M_{BH} = 10^{-3} M_*$, in agreement with the Magorrian et al. (1998) relation. The dark halo has a Navarro et al. (1997; NFW) profile $[\rho_h \propto 1/(r/r_h)(1+r/r_h)^2]$, with r_h the scale radius, and truncated at large radii, and a total mass M_h . For each σ_c , the defining parameters of the stellar mass model were chosen accordingly to the observational constraints that L_B follows the Faber-Jackson relation, and that L_B , σ_c and the effective radius R_e lie on the Fundamental Plane of ETGs (e.g., Bernardi et al. 2003). The free parameters defining the dark matter were chosen in agreement with the results from dynamical modeling of the observed motions of stars, planetary nebulae and globular clusters at small and large radii; these indicate that the dark matter begins to be dynamically important at $2-3R_e$ (e.g., Saglia et al. 1992, Cappellari et al. 2006, Weijmans et al. 2009, Shen & Gebhardt 2010). This requires that $\beta = r_h/R_e > 1$, and $\mathcal{R} = M_h/M_* = 3$ or 5 (the latter value corresponding to the baryon-to-total mass ratio of WMAP, Komatsu et al. 2009). By solving numerically the Jeans equations for the three mass components in the isotropic orbits case (e.g., Binney & Tremaine 1987), these choices produce M_* , M_h and \mathcal{R}_e (the dark-to-luminous mass ratio within R_e). Reasonable values of $M_*/L_B = (4-10) M_\odot/L_{B,\odot}$, and $\mathcal{R}_e = 0.2-1.0$ are obtained. The main properties of a few representa-

² For example, we recall two approximations made here with respect to the case of real ETGs: the total gas profile may be different from that of the stars, and the flow has a time-continuous distributed mass and energy input. The first of these points will be further discussed in Sect. 5.

tive mass models are shown in Fig. 1.

For a consistent comparison between observed T 's and the characteristic temperatures derived for the mass models, the central stellar velocity dispersion σ_c must be the same for observed ETGs and models. Typically, for nearby well observed ETGs, the value of σ_c is that of the projected and luminosity-weighted average within an aperture of radius $R_e/8$. Therefore, when defining a mass model, the chosen value of σ_c was assigned to this quantity. Finally, streaming motions as stellar rotation are not considered in these models (possible heating from these motions is discussed by Ciotti & Pellegrini 1996).

5. DISCUSSION

We investigate here the relationship between the observed T 's and those expected from the various sources of heating (stellar motions, gravitational potential, SNIa's), or during the escape of the hot gas. For this purpose, Fig. 2 shows the run with σ_c of the various temperatures defined in Sects. 2.2, 2.3, and 3, together with the distribution of the observed T values from BKF (Sect. 1); for the BKF sample, the value of σ_c is the luminosity weighted average within $R_e/8$, and has been taken from SAURON studies for 12 ETGs (Kuntschner et al. 2010), for the remaining cases from the references in the Hyperleda catalog (see Tab. 1).

The temperatures defined in Sects. 2.2, 2.3, and 3 are mass-weighted averages, which is required when discussing energetic aspects of the gas (e.g., the energy required for escape as measured by $\langle T_{\text{grav}}^- \rangle$ compared with the input energy from SNIa's). When a direct comparison is made with observed T 's, it must be noted that the latter coincide with mass-weighted averages only if the ISM has everywhere one single temperature value; if the gas is multi-phase, or its temperature profile has a gradient, a single T value measured from the spectrum of the integrated emission will be close to an emission-weighted average (e.g., Ciotti & Pellegrini 2008, Kim 2011). This means that, since the densest region is the central one, the measured T 's tend to be closer to the central values than the mass-weighted ones. The temperature profiles observed with *Chandra* change continuously in shape, as the emission-weighted average T decreases from $\lesssim 1$ keV to ~ 0.3 keV: they switch from a flat central profile that increases outward of $\sim 0.5R_e$, to a quasi-isothermal profile, to a profile with a negative gradient (Diehl & Statler 2008, Nagino & Matsushita 2009). Therefore, the lowest observed T 's, presumably associated with the last category, may be larger than mass-weighted values, intermediate T 's may be the closest to mass-weighted averages, while the largest observed T 's may be lower than mass-weighted averages. Another aspect to recall is that the temperatures defined in Sects. 2.2, 2.3, and 3 refer to a gas distribution with $\rho_{\text{gas}} \propto \rho_*$; this is appropriate for the continuously injected gas (e.g., for $\langle T_{\text{inj}} \rangle$), while it may be less accurate when comparing observed T 's with $\langle T_{\text{esc}}^{\text{sub}} \rangle$, or when discussing the energetics of the whole gas content of an ETGs by means of $\langle T_{\text{grav}}^+ \rangle$ and $\langle T_{\text{grav}}^- \rangle$, since the bulk of the hot ISM may have a different distribution from the stars. For example, the observed X-ray brightness profile of gas-rich ETGs was found to follow the optical one, which was taken as evidence that roughly

$\rho_{\text{gas}} \propto \sqrt{\rho_*}$ (e.g., Sarazin & White 1988, Fabbiano 1989). For gas-poor ETGs hosting galactic winds, the modeling shows that the profile $\rho_{\text{gas}}(r)$ will again be shallower than $\rho_*(r)$, though not as much as in the previous case (see, e.g., White & Chevalier 1983). If ρ_{gas} has a flatter radial profile than ρ_* , then it is easy to show that its mass-weighted $\langle T_{\text{grav}}^+ \rangle$ will be larger than derived using Eq. 4, and its mass-weighted $\langle T_{\text{grav}}^- \rangle$ and $\langle T_{\text{esc}}^{\text{sub}} \rangle$ will be lower than derived using Eqs. 6 and 7. In conclusion, the comparison of observed T 's with mass-weighted expectations is the best that can be done currently, in a general analysis as that of the present work, though with the warnings above. Note, however, that all arguments and conclusions below remain valid or are strengthened, when taking into account the above considerations about observed T 's, or about the modifications to $\langle T_{\text{grav}}^+ \rangle$, $\langle T_{\text{grav}}^- \rangle$ and $\langle T_{\text{esc}}^{\text{sub}} \rangle$.

5.1. Observed and predicted temperatures in the $T - \sigma_c$ plane

In the left panel of Fig. 2 the observed T 's are compared with approximate estimates of the stellar temperature T_σ , of T_{inj} , and of the escape temperature $4T_\sigma$ (Sect. 3). The gas luminosity is also indicated with different colors, having grouped the L_X values in three ranges, chosen to have a roughly equal number of ETGs in each range. This grouping gives an indication of the gas flow status, based on previous works: a galactic wind leaving the galaxy with a supersonic velocity has $L_X < 10^{38}$ erg s^{-1} (e.g., Mathews & Baker 1971, Trinchieri et al. 2008), global subsonic outflows and partial winds can reach $L_X \sim 10^{40}$ erg s^{-1} (Ciotti et al. 1991, Pellegrini & Ciotti 1998), and a central inflow becomes increasingly more important in ETGs of increasingly larger L_X . Magenta ETGs (10^{38} erg $\text{s}^{-1} < L_X < 1.5 \times 10^{39}$ erg s^{-1}) should then host winds, subsonic outflows, and partial winds with a very small inflowing region of radius < 100 pc; cyan ETGs (1.5×10^{39} erg $\text{s}^{-1} < L_X < 1.2 \times 10^{40}$ erg s^{-1}) should host subsonic outflows and partial winds with an increasingly larger inflowing region (of radius up to a few hundreds pc); black ETGs are hot gas-rich and mostly inflowing³. The best fit found for X-ray bright ETGs is also shown in the left panel (O'Sullivan et al. 2003), and gives a good representation of the distribution of observed T 's down to a range of low temperatures and gas contents never explored before. The slope of the fit ($T \propto \sigma_c^{1.79}$) and that of the $T_\sigma \propto \sigma_c^2$ relation are similar, with the fit being shallower; this could be due to the fact that not all heating sources depend on σ_c^2 , see, e.g., the important SNIa's contribution in T_{inj} , that produces a much flatter run of T_{inj} with σ_c (Fig. 2). The fit was mostly based on gas-rich ETGs, whose T 's show a trend with σ_c closer to that of T_σ (an aspect further addressed

³ In the X-ray faintest ETGs, the gas emission L_X is $\sim (1 - 2)$ times the integrated emission from the population of weak unresolved stellar sources (Sect. 1), generally referred to as AB+CVs. BKF derived an AB+CV emission model by jointly fitting the M31 and M32 spectra, and then tested how the measurement of the gas properties may be affected by the adopted AB+CV model (their Sect. 3.1). By fitting with different AB+CV models, all within the uncertainties in the adopted one, the measured T changed only negligibly, for the 6 lowest- L_X ETGs of their sample; a systematic uncertainty of 10% - 20% was found for the gas flux (much lower for the X-ray brighter ETGs).

below in Sects. 5.2 and 6), while gas-poor ETGs depart most from it, since their T 's change little for largely varying σ_c (as found by BKF; see Sect. 5.4 below).

The right panel of Fig. 2 shows the stellar temperature $\langle T_* \rangle$, the injection temperature $\langle T_{inj} \rangle$, the escape temperature $\langle T_{grav}^- \rangle$, and the characteristic temperature for slowly outflowing gas $\langle T_{esc}^{sub} \rangle$, calculated for a set of representative galaxy mass models (Sect. 4). At any fixed σ_c and Sérsic index n , $\langle T_* \rangle$, $\langle T_{grav}^- \rangle$ and $\langle T_{esc}^{sub} \rangle$ are larger for larger galaxy mass (\mathcal{R}), and mass concentration (smaller β)⁴. The dashed lines represent a reasonable upper limit to the values of each of the characteristic temperatures, since they correspond to the most massive model ETGs, with the most concentrated dark matter allowed for by recent studies (Sect. 4). The $\langle T_{grav}^- \rangle$ curves lie below the simple approximation of the escape temperature given by $4T_\sigma$; $\langle T_{grav}^- \rangle = 4.8 \langle T_* \rangle$, for $\mathcal{R} = 3$, and $\simeq 5.2 \langle T_* \rangle$, for the three cases with $\mathcal{R} = 5$.

As expected, all the $\langle T_* \rangle$ curves lie below T_σ , that overestimates the kinetic energy associated with the stellar random motions (Sect. 2.2). Note that, from the virial theorem, $\langle T_* \rangle$ is independent of orbital anisotropy, that just redistributes differently the stellar heating within a galaxy; the presence of ordered rotation in the stellar motions, instead, requires a more careful consideration. For any fixed galaxy mass model, this rotation would leave the total stellar heating unchanged or lower it, depending on whether the whole stellar streaming motion is converted into heat, or just a fraction of it (Ciotti & Pellegrini 1996). For the worst case that the stellar rotational motion is not thermalized at all, and the galaxy is a flat isotropic rotator, $\langle T_* \rangle$ in Fig. 2 should be an overestimate of $\sim 30\%$ of the temperature corresponding to the stellar heating (Ciotti & Pellegrini 1996); the possible reduction of $\langle T_* \rangle$ to be considered should be lower than this, as far as the massive ETGs in Fig. 2 are less flattened and more pressure supported systems (e.g., Emsellem et al. 2011).

All observed T 's are located above $\langle T_* \rangle$; thus, additional heating with respect to the thermalization of the stellar kinetic energy is needed, as noticed previously using T_σ (e.g., Davis & White 1996, BKF). The gas could retain memory of its injection temperature, and have the additional infall heating, as examined in Sects. 5.2 and 5.3 below.

Finally, the values of $\langle T_{inj} \rangle$ for $f = 0.85$ are by far the largest temperatures of Fig. 2, larger than $\langle T_{grav}^- \rangle$ up to $\sigma_c \sim 250 \text{ km s}^{-1}$; therefore, SNIa's should cause the escape of the gas for all ETGs up to this σ_c , since the gas at every time is injected with an energy larger than required to leave the galaxy potential. This expectation is fulfilled by all ETGs with $\sigma_c \lesssim 200 \text{ km s}^{-1}$: their X-ray properties (a low L_X , and T 's of the order of $\langle T_{esc}^{sub} \rangle$) agree well with what expected if outflows are important in them. This result had been suggested previously based on the low observed L_X ; now for the first time it can be confirmed based on the observed T values. At $\sigma_c > 200 \text{ km s}^{-1}$, instead, ETGs may have L_X far larger than

⁴ All the rest equal, these temperatures are also larger for smaller n , due to the galaxy being more massive to reproduce the same σ_c , since the stellar mass profile is less steep (e.g., Fig. 1).

expected for outflows (black symbols), and most ETGs where likely outflows are important (magenta or cyan symbols) have T much lower than $\langle T_{esc}^{sub} \rangle$; these findings are discussed in Sect. 5.4 below.

5.2. Gravitational heating in gas-rich ETGs

We examine here the possibility that the additional heating with respect to the thermalization of the stellar kinetic energy is provided by infall heating and SNIa's. Davis & White (1996) assumed that in all ETGs the hot gas is inflowing, and suggested that the observed temperatures are larger than T_σ just due to the luminous parts of ETGs being embedded in dark matter halos dynamically hotter than the stars; i.e., a form of "gravitational potential" way for the gas heating was invoked. This way can consist of an effect of the dark halo on the stellar motions, that are then thermalized, or directly on the gas during infall (e.g., via E_{grav}^+). The first possibility is excluded by the $\langle T_* \rangle$ curves in Fig. 2, that are always lower than T_σ , and that, through the Jeans equations, include the effect of a massive dark halo consistent with the current knowledge of the ETGs' structure. In the second possibility of heating from gas infall, E_{grav}^+ is indeed potentially an important source of heating, that increases with the amount and concentration of the dark matter. This can be judged from Fig. 2, after considering that $\langle T_{grav}^- \rangle \sim 5 \langle T_* \rangle$, and that the temperature possibly attainable from infall was estimated to be $T_{infall} \lesssim \langle T_{grav}^- \rangle$ (end of Sect. 3). Note that T_{infall} (if it behaves as $\langle T_{grav}^+ \rangle$) could be $\propto \sigma_c^2$, a trend close to that shown by the T 's of gas-rich ETGs (BKF; see also Sect. 6 below).

Inflowing ETGs can also benefit of the SNIa's energy input; for the unit mass of injected gas, this is written as $E_{SN}^{tot} = R_{SN} E_{SN} / \dot{M}_*$. Both E_{grav}^+ and E_{SN}^{tot} then contribute to the required additional thermal energy with respect to that gained from the stellar random motions, i.e., to $\Delta E_{th} = 3k(T - \langle T_* \rangle) / 2\mu m_p$. E_{grav}^+ and E_{SN}^{tot} can be in large part radiated in gas-rich ETGs, but they seem to far exceed the required ΔE_{th} . For example, for the highest- L_X of Fig. 2, $\Delta E_{th} \sim (1 - 2) \times 10^{48} \text{ erg } M_\odot^{-1}$ (i.e., $\sim 0.2 - 0.4 \text{ keV}$), when adopting an average galaxy mass model as that of the thick black line in Fig. 2. The energy spent in radiation can be estimated, in a stationary situation, as L_X / \dot{M}_* (per unit injected gas mass); using L_X from BKF and deriving \dot{M}_* as in Sect. 2.1, for the same distances in BKF and galactic B-magnitudes given by Hyperleda, for the gas-rich ETGs one finds that L_X / \dot{M}_* ranges between $(0.5 - 3.4) \times 10^{48} \text{ erg } M_\odot^{-1}$. The energy available is far larger than the sum of ΔE_{th} and L_X / \dot{M}_* : $E_{SN}^{tot} = 7.3 \times 10^{48} (f/0.85) \text{ erg } M_\odot^{-1}$, and $0.5 E_{grav}^+$ ranges from $4 \times 10^{48} \text{ erg } M_\odot^{-1}$ ($\sigma_c \sim 220 \text{ km s}^{-1}$) to $8 \times 10^{48} \text{ erg } M_\odot^{-1}$ ($\sigma_c \sim 300 \text{ km s}^{-1}$), for the mass model with the thick black line in Fig. 2. These results are detailed in Fig. 3, where the values of ΔE_{th} and L_X / \dot{M}_* for each galaxy are shown, together with various combinations of E_{grav}^+ and E_{SN}^{tot} . In conclusion, additional input energy for the gas to account for the observed T 's of gas-rich ETGs seems available in a sufficient amount, even if f were to be < 0.85 .

5.3. Outflows and SNIa's heating

The gas is not mostly inflowing in all ETGs, while it is hotter than $\langle T_* \rangle$ in all of them. When in outflow, the radiative losses are far smaller, but energy is spent in extracting the gas from the galaxy and giving it a bulk velocity. We discuss here the possibility of heating from the SNIa's energy input to account for the observed ΔE_{th} of ETGs where outflows are likely important (those with low/medium L_X , magenta and cyan symbols in Fig. 2).

We assume that the SNIa's energy is used for the uplift of the gas and the kinetic energy with which it escapes from the galaxy, and, neglecting radiative losses, that all the remaining part is available to account for the observed ΔE_{th} . Then, the energy balance per unit mass of injected gas is $E_{SN}^{tot} = E_{grav}^- + E_{out} + \Delta E_{th}$, where ΔE_{th} is the same as in Sect. 5.2, and $E_{out} = v_{out}^2/2$ is the mass-averaged kinetic energy of the escaping material per unit gas mass. Figure 4 shows ΔE_{th} derived from this balance, for $v_{out} = c_s$, and c_s calculated for $\gamma = 5/3$ and $kT = 0.3$ keV, a temperature of the order of that observed for ETGs likely in outflow (Fig. 2). Adopting $v_{out} \sim c_s$ (independent of σ_c) produces an E_{out} on the upper end of those expected⁵, and then the estimate of ΔE_{th} may be biased low. With $v_{out} \sim c_s$, E_{out} is just $\sim 0.1(f/0.85)E_{SN}^{tot}$. The energy needed for gas extraction E_{grav}^- , for the same galaxy mass model used in Sect. 5.2, varies instead from $\sim 1/3(f/0.85)E_{SN}^{tot}$ for $\sigma_c = 150$ km s⁻¹, to $\sim E_{SN}^{tot}$ for $\sigma_c = 250$ km s⁻¹; this explains the strong dependence of the predicted ΔE_{th} on σ_c in Fig. 4. It is clear from this figure that for $f = 0.85$ SNIa's can account for the needed heating in all ETGs with low/medium L_X ; for $f = 0.35$, instead, the temperature increase would fall short of what required for all ETGs. In Fig. 4, the energy losses due to radiation are also shown; their small size supports the hypothesis that in most cases they do not affect significantly the energy budget of the gas.

Given the flat distribution of the observed points in Fig. 4, and the steep behavior of the curves predicting ΔE_{th} , the value of f required to account for the observed ΔE_{th} increases with σ_c . In particular, the value of $f \sim 0.85$ that is required at high σ_c would produce an expected ΔE_{th} at low σ_c that is larger than observed. A possible solution could reside in the efficiency of the SNIa's energy mixing process. In massive, gas-rich ETGs, SNIa's bubbles should disrupt and share their energy with the local gas within $\sim 3 \times 10^6$ yr (Mathews 1990); for a Milky Way-size bulge in a global wind, instead, 3D hydrodynamical simulations of discrete heating from SNIa's suggest a non-uniform thermalization of the SNIa's energy, with overheated gas by a SNIa explosion at the bulge center that is advected outwards, carrying a large fraction of the SNIa energy with it (Tang et al. 2009). For subsonic outflows the mixing is expected to be more local and more complete (Lu & Wang 2011). The magenta and cyan ETGs in Fig. 4 have gas densities and luminosities larger than those considered by

⁵ For example, in a wind solution, the terminal (i.e., the largest) velocity of the flow is roughly the central sound speed (White & Chevalier 1983); moreover, in this solution the gas is likely to be already too "fast" with respect to that of most magenta ETGs in Fig. 2, due to their L_X (e.g., Trinchieri et al. 2008).

Tang et al. (2009); however, if a discrete heating effect were still present at $\sigma_c < 200$ km s⁻¹, it could qualitatively explain a lower f for these galaxies. There is also the possibility that $\langle T_* \rangle$ has been overestimated (and then the observed ΔE_{th} underestimated) at the low σ_c , if these ETGs are less pressure supported systems (e.g., Emsellem et al. 2011), and the stellar rotational streaming is not all thermalized (Sect. 5.1). Another possible explanation could be that ETGs with $\sigma_c > 200$ km s⁻¹ are less outflow-dominated than those at lower σ_c (though this is not supported just based on L_X , since magenta ETGs are found over the whole σ_c range in Fig. 4), so that their E_{grav}^- would be lower than assumed by the curves in Fig. 4, and more SNIa's energy would be available for heating. In this way, f could have a value < 0.85 , possibly similar for all ETGs.

Finally, a comparison of Figs. 3 and 4 shows that the average ΔE_{th} is slightly larger for the X-ray brightest ETGs (for which it ranges between 0.1–0.5 keV) than for the X-ray faintest ones (0–0.3 keV); moreover, while the ΔE_{th} in Fig. 3 can be explained even with $f < 0.85$, it is required that $f \sim 0.85$ for the X-ray faintest ETGs with the largest σ_c in Fig. 4. Both facts are the consequence of the large fraction of the SNIa's energy input that is used in gas extraction where outflows dominate, while all the SNIa's energy remains within the galaxies where inflow dominates.

In conclusion, even for ETGs with low/medium L_X , a fundamental X-ray property as T can be accounted for by simple arguments, just based on realistic galaxy mass models, and reasonable SNIa's heating capabilities. There may be, though, more energy available for the gas in ETGs with $\sigma_c < 200$ km s⁻¹ than can be accounted for by the present simple scenario.

5.4. The temperature and gas flows status in ETGs of intermediate mass

The observed X-ray properties (low L_X and $T \sim \langle T_{esc}^{sub} \rangle$), and the energy budget of the gas (e.g., $\langle T_{grav}^- \rangle$ vs. $\langle T_{inj} \rangle$), for ETGs with $\sigma_c \lesssim 200$ km s⁻¹ are all consistent with the expectations for outflows; the large L_X and $\langle T_{grav}^- \rangle$ larger than $\langle T_{inj} \rangle$ of ETGs with $\sigma_c > 250$ km s⁻¹ agree with the gas being mostly inflowing. For $200 < \sigma_c$ (km s⁻¹) < 250 , instead, ETGs show very different L_X and T , whose values seem unrelated to $\langle T_{esc}^{sub} \rangle$ and to the relative size of $\langle T_{grav}^- \rangle$ and $\langle T_{inj} \rangle$ (Fig. 2). For example, for $f = 0.85$, $\langle T_{inj} \rangle$ exceeds $\langle T_{grav}^- \rangle$, but most T values lie well below $\langle T_{esc}^{sub} \rangle$, and even high L_X values (incompatible with outflows) are common. One first explanation could be that $f < 0.85$; for example, for $f = 0.35$, $\langle T_{inj} \rangle$ becomes lower than $\langle T_{grav}^- \rangle$ at $\sigma_c \sim 180$ km s⁻¹ (Fig. 2). Four ETGs with $\sigma_c > 200$ km s⁻¹ and a very low L_X (Fig. 2, magenta symbols), though, require that $f > 0.35$ in them, and then that f varies from galaxy to galaxy, or that their gas was removed by other processes as an AGN outburst (e.g., Machacek et al. 2006, Ciotti et al. 2010), or a merging or an interaction (Read & Ponman 1998, Sansom et al. 2006, Brassington et al. 2007). An event like the latter two in the recent past is unlikely for three of these ETGs (NGC1023, NGC3115, NGC3379), that are very regular in their stellar morphological and kine-

matic properties, while in the other ETG (NGC4621) that hosts a counter-rotating core (Wernli et al. 2002) it is possible.

A second explanation could be that $\langle T_{inj} \rangle$ exceeds $\langle T_{grav}^- \rangle$ only at the present epoch: while $\langle T_* \rangle$ and $\langle T_{grav}^- \rangle$ are independent of time, T_{SN} may have been lower in the past (Eq. 1), to the point that $\langle T_{inj} \rangle$ may have been lower than $\langle T_{grav}^- \rangle$ for more ETGs than in Fig. 2 (that represents a snapshot of the present epoch). The gas then could have accumulated and radiative losses have become important, even for the gas injected in later epochs. In fact, the population synthesis models of Sect. 2 predict that \dot{M}_* was larger at early times (e.g., by ~ 6 times at an age of 3 Gyr), and then to keep T_{SN} high in the past, from Eq. 1, \dot{M}_{SN} must decrease with time t at a rate similar to or steeper than that of the stellar mass losses ($\dot{M}_* \propto t^{-1.3}$; Ciotti et al. 1991). Recent observational estimates indicate instead a SNIa's rate decaying close to t^{-1} (Maoz et al. 2010, Sharon et al. 2010), thus T_{SN} and $\langle T_{inj} \rangle$ should be increasing with time, reaching the values of Fig. 2 at the present epoch. Then, a ‘‘cooling effect of the past’’ would explain a moderate or high L_X even where $\langle T_{inj} \rangle$ exceeds $\langle T_{grav}^- \rangle$ in Fig. 2.

Both explanations, $f < 0.85$ and/or a lower $\langle T_{inj} \rangle$ in the past, can account for the lack of a widespread presence of outflows for $200 < \sigma_c (\text{km s}^{-1}) < 250$. Both, though, require a mechanism different from the SNIa's energy input to cause degassing in some low L_X ETGs in the same σ_c range.

Another possibility is that partial winds become common for $\sigma_c > 200 \text{ km s}^{-1}$: these ETGs host an inner inflow and an outer outflow (e.g., MacDonald & Bailey 1978), with variations in the galactic structure causing different sizes for the inflowing region, and then different L_X (Pellegrini & Ciotti 1998). This possibility holds even for $f = 0.85$, and for both kinds of time evolution of $\langle T_{inj} \rangle$; in fact, if the flow is decoupled, ETGs may host a central inflow even if $\langle T_{inj} \rangle$ is larger than $\langle T_{grav}^- \rangle$. Similarly, the observed T 's can be lower than $\langle T_{esc}^{sub} \rangle$, in ETGs where the outflow is only external; in this case, the observed T 's may also be lowered by radiative losses in the central inflowing region.

6. THE TEMPERATURE OF INFLOWS AND OUTFLOWS

In Fig. 2, the hottest gas is in ETGs with the highest L_X , and the coolest one in ETGs with the lowest L_X (as also found by BKF). This feature is also present in the $L_X - \sigma_c$ relation, where ETGs with $kT > 0.4 \text{ keV}$ are the X-ray brightest (with one exception), while those with $kT < 0.3 \text{ keV}$ are the X-ray faintest (BKF). All this may seem contrary to the simple expectation that hotter gas is needed for escape, and that the hotter the gas, the stronger the outflow, the lower the gas content. We re-examine below this point, first across the whole σ_c range, and then at fixed σ_c .

A proper consideration of whether outflowing ETGs possess hotter or colder gas than inflowing ones requires that all T 's are rescaled by a temperature equivalent to the depth of the potential where the gas resides (for example, by T_σ). Is there a trend then of the distance of the observed T 's from $\langle T_{esc}^{sub} \rangle$, or $\langle T_* \rangle$? This is

examined by Fig. 5, where temperatures are rescaled by T_σ , and the σ_c^2 dependency of all the curves in Fig. 2 is removed. Figure 5 shows that for $\sigma_c < 200 \text{ km s}^{-1}$ the observed points reach $\langle T_{esc}^{sub} \rangle / T_\sigma$, a result similar to that of Fig. 2, and that they fall below it with increasing σ_c (with a transition region of large dispersion in T/T_σ). Therefore ETGs with $\sigma_c < 200 \text{ km s}^{-1}$ are indeed the hottest, relatively to the virial temperature; since in these ETGs outflows are important (Sect. 5.1), indeed the flow is relatively hotter in outflows, and T increases going from outflows to inflows only in an absolute sense. The T 's of the X-ray brightest ETGs should show a dependence on σ_c^2 , if gravitational heating of the gas dominates over SNIa's heating, and then they should lie within a horizontal zone in Fig. 5. The observed distribution does not disagree with this kind of dependence, but more cases are needed to firmly establish its presence; such a dependence is not expected, though, since the SNIa's heating should easily dominate over the gravitational one (Sect. 5.2).

We finally compare the T 's at similar σ_c , in the most populated region of Fig. 5, for $200 < \sigma_c (\text{km s}^{-1}) < 250$. Here the variation of T/T_σ is the largest, and is covered by ETGs of all X-ray emission levels; the X-ray brightest ETGs are found at $T/T_\sigma > 1.1$, while the lowest T/T_σ values belong to the X-ray fainter ETGs. For example, two of the three lowest T/T_σ values of the figure (those of NGC3379 and NGC4621) belong to the X-ray faintest group. While heating sources seem abundant in gas-rich ETGs to account for their T 's (see, e.g., Fig. 3, and the additional possibility of MBH heating, Sect. 2.4), even after taking into account their radiative losses, this result remains more difficult to explain for ETGs of low/medium L_X , and may require ad hoc solutions. It may be another representation of what mentioned in Sect. 5.3, that ΔE_{th} can be larger for the X-ray brightest ETGs than for the X-ray faintest ones, due to the different employment of the SNIa's input energy; or it could be that $f < 0.85$ in these ETGs so that SNIa's cannot make their gas hotter than this (Fig. 4); or their galaxy structure may be much different from an average one, so that dividing all T 's for the same T_σ produces a biased view; or the evolutionary history of the gas may have been peculiar. Certainly, this trend needs further investigation and, if confirmed, it will provide the basis for further theoretical work.

7. CONCLUSIONS

This work has focussed on the origin of the hot gas temperatures recently derived for a sample of ETGs observed with *Chandra* down to galaxy masses and X-ray luminosities smaller than ever before. A few characteristic mass-weighted average temperatures have been defined for a gas distribution $\rho_{gas}(r) \propto \rho_*(r)$, as for the gas shed by stars: the virial temperature $\langle T_* \rangle$; the injection temperature $\langle T_{inj} \rangle$, as the sum of $\langle T_* \rangle$ and of a temperature equivalent to the SNIa's kinetic energy input (with a factor f allowing for its uncertain thermalization); the escape temperature $\langle T_{grav}^- \rangle$, defined as the temperature equivalent of the energy required for escape from the gravitational potential; a fiducial value for the temperature of escaping gas, evaluated on a streamline of very subsonic velocity ($\langle T_{esc}^{sub} \rangle = 0.6 \langle T_{grav}^- \rangle$);

and finally, the temperature equivalent to the energy liberated by the gas inflow to the galactic center, $\langle T_{\text{grav}}^+ \rangle$. These temperatures were then calculated for a set of representative galaxy mass models, made by the superposition of a central MBH, and a stellar and a dark mass density distributions, with parameters constrained from the fundamental scaling laws of ETGs and recent observational findings. The main properties of the characteristic temperatures are that:

- All temperatures scale as σ_c^2 (except for $\langle T_{\text{inj}} \rangle$), and increase for larger and/or more concentrated mass content. For the adopted set of representative galaxy mass models, $\langle T_* \rangle$ is lower than T_σ (by $\sim 0.1 - 0.2$ keV), $\langle T_{\text{grav}}^- \rangle \approx 5 \langle T_* \rangle$, and $\langle T_{\text{grav}}^+ \rangle \approx 2 \langle T_{\text{grav}}^- \rangle$; the temperature that can be produced by infall heating, though, will be much lower than $\langle T_{\text{grav}}^- \rangle$, due to energy losses in radiation, kinetic energy of mass condensations, and mass drop-outs from the flow.

- $\langle T_{\text{inj}} \rangle$ is by far the largest of the characteristic temperatures, due to the important SNIa's contribution (independent of σ_c); for $f = 0.85$, it is larger than the minimum injection temperature for global escape up to $\sigma_c \sim 250 \text{ km s}^{-1}$.

The comparison of the characteristic temperatures with those observed, in the $T - \sigma_c$ plane, shows that:

- The best fit $T - \sigma_c$ relation previously found for X-ray bright ETGs reproduces the average trend of the observed T down to low temperatures, and low L_X . ETGs with low/medium L_X show the largest departures from this fit, which can be explained by the variety of gas flow phases possible in them (winds, subsonic outflows, partial winds), where the main input energies (from SNIa's and gas infall) are used in different ways.

- All observed T 's are larger than $\langle T_* \rangle$; the additional heating of the gas ΔE_{th} , with respect to that provided by the thermalization of the stellar motions, is $\Delta E_{\text{th}} \approx 0 - 0.3$ keV for the X-ray faintest ETGs, and $\Delta E_{\text{th}} \approx 0.1 - 0.5$ keV for the X-ray brightest (for a representative galaxy mass model).

- In a stationary situation, ΔE_{th} of the X-ray brightest ETGs can be accounted for by the energy input of SNIa's and gas infall, even if they are much reduced with respect to standard assumptions (i.e., f can be < 0.85). The gravitational heating produces a $T \propto \sigma_c^2$ trend, that may be present in the X-ray brightest ETGs; the SNIa's heating, though, is expected to be dominant.

- ΔE_{th} can be provided by SNIa's in X-ray fainter ETGs, where outflows are important; most of the SNIa's energy is needed for gas extraction, and less for the kinetic energy of the escape. The value of f to account for the observed ΔE_{th} increases with σ_c , until the whole SNIa's energy ($f \approx 0.85$) is required at the highest σ_c . With this f , though, at low σ_c the observed ΔE_{th} are lower than expected. Possible solutions require a different efficiency of the SNIa's energy mixing process, or an overestimate of $\langle T_* \rangle$ at low σ_c if these ETGs are less pressure supported systems, or a more complex flow status than in the simple scheme adopted.

- At low $\sigma_c \lesssim 200 \text{ km s}^{-1}$, $\langle T_{\text{inj}} \rangle$ is larger than $\langle T_{\text{grav}}^- \rangle$, the L_X values are low and the T 's are of the order of $\langle T_{\text{esc}}^{\text{sub}} \rangle$: all this agrees well with what expected for outflows. At high $\sigma_c > 250 \text{ km s}^{-1}$,

$\langle T_{\text{inj}} \rangle$ is lower than $\langle T_{\text{grav}}^- \rangle$, and the high L_X and T can be explained with the gas mostly inflowing. For $200 < \sigma_c (\text{km s}^{-1}) < 250$, instead, there is a large variation in L_X and T . Possible explanations could be that the SNIa's energy input varies from galaxy to galaxy, and/or that $\langle T_{\text{inj}} \rangle$ was lower in the past, due to the different time evolution of the mass loss and the SNIa's rate; or that partial winds become common, with the flow status less related to the values of $\langle T_{\text{inj}} \rangle$, $\langle T_{\text{grav}}^- \rangle$, and $\langle T_{\text{esc}}^{\text{sub}} \rangle$.

- When measured relatively to the depth of the potential well, the observed temperatures T/T_σ are larger for $\sigma_c < 200 \text{ km s}^{-1}$ (outflows), and lower for $\sigma_c > 250 \text{ km s}^{-1}$ (inflows). The observed T 's then increase from outflows to inflows only in an absolute sense, and the gas is relatively hotter in outflows. In the intermediate region of $200 < \sigma_c (\text{km s}^{-1}) < 250$, lower L_X values tend to correspond to lower T and T/T_σ , which requires ad hoc explanations, and then deserves further observational and theoretical investigation.

I thank Luca Ciotti for helpful discussions, and Dong-Woo Kim and the referee for useful comments.

REFERENCES

- Athey, A., Bregman, J., Bregman, J., Temi, P., Sauvage, M., 2002, *ApJ*, 571, 272
- Auger, M.W., Treu, T., Bolton, A.S., et al. 2010, *ApJ* 724, 511
- Bender, R., Saglia, R.P., Gerhard, O.E., 1994, *MNRAS* 269, 785
- Bernardi, M., Sheth, R. K., Annis, J. B., et al., 2003, *AJ*, 125, 1866
- Binney, J., Tremaine, S., *Galactic Dynamics*, PUP (1987)
- Binney, J., Davies, R.L., Illingworth, G.D., 1990, *ApJ*, 361, 78
- Birzan, L., Rafferty, D. A., McNamara, B. R., Wise, M. W., Nulsen, P.E.J. 2004, *ApJ* 607, 800
- Borson, B., Kim, D.W., Fabbiano, G., 2011, *ApJ* 729, 12
- Brassington, N. J., Ponman, T.J., Read, A.M., 2007, *MNRAS*, 377, 1439
- Brown, B. A., Bregman J. N., 2000, *ApJ*, 539, 592
- Cappellari, M., Bacon, R., Bureau, M., et al. 2006, *MNRAS*, 366, 1126
- Cappellaro, E., Evans, R., Turatto, M., 1999, *A&A*, 351, 459
- Chevalier, R.A., 1974, *ApJ* 188, 501
- Ciotti L., D'Ercole A., Pellegrini S., Renzini A. 1991, *ApJ* 376, 380
- Ciotti, L., Pellegrini, S., 1992, *MNRAS*, 255, 561
- Ciotti, L., Pellegrini, S., 1996, *MNRAS*, 279, 240
- Ciotti, L., Pellegrini, S., 2008, *MNRAS*, 387, 902
- Ciotti, L., Ostriker, J. P., Proga, D. 2010, *ApJ*, 717, 708
- David, L. P., Forman, W., Jones, C., 1990, *ApJ*, 359, 29
- David, L.P., Jones, C., Forman, W., Vargas, I.M., Nulsen, P., 2006, *ApJ* 653, 207
- Davis, D.S., White, R.E.III, 1996, *ApJ* 470, L35
- Diehl, S., & Statler, T. S., 2007, *ApJ*, 668, 150
- Diehl, S., & Statler, T. S., *ApJ*, 687, 986 (2008)
- D'Onofrio, M., Zaggia, S., Longo, G., Caon, N., Capaccioli, M., 1995, *A&A* 296, 319
- Emsellem, E., et al. 2011, in press on *MNRAS* (arXiv:1102.4444)
- Eskridge, P. B., Fabbiano, G., Kim, D.-W., 1995, *ApJS* 97, 141
- Fabbiano, G., 1989, *ARA&A*, 27, 87
- Fabbiano, G., 2006, *ARA&A*, 44, 323
- Fisher, D., 1997, *AJ*, 113, 950
- Fukazawa, Y., Botoya-Nonesa, J.G., Pu, J., Ohto, A., Kawano, N., 2006, *ApJ*, 636, 698
- Gallo, E., Treu, T., Marshall, P.J., Woo, J.-H., Leipski, C., Antonucci, R. 2010, *ApJ* 714, 25
- Gisler, G.R., 1976, *A&A* 51, 137
- Kim, D.W., 2011, in *Hot Interstellar Matter in Elliptical Galaxies*, eds. D.W. Kim and S. Pellegrini, Astrophysics and Space Science Library, Springer (NY), in press

- Komatsu, E., Dunkley, J., Nolta, M. R., et al., 2009, *ApJS*, 180, 330
- Kormendy, J., Fisher, D.B., Cornell, M.E., Bender, R. 2009, *ApJS* 182, 216
- Kuntschner, H., Emsellem, E., Bacon, R., et al. 2010, *MNRAS* 408, 97
- Larson, R.B., 1974, *MNRAS* 166, 585
- Li, et al. 2010, *ApJin press*, arXiv:1006.4613
- Loewenstein, M., Mathews, W.G., 1987, *ApJ*, 319, 614
- Longo, G., Zaggia, S., Busarello, G., Richter, G., 1994, *A&AS* 105, 433
- Lu, Z., Wang, Q.D., 2011, *MNRAS* 413, 347
- MacDonald, J., Bailey, M. E., 1981, *MNRAS*, 197, 995
- Machacek, M., Nulsen, P. E. J., Jones, C., Forman, W. R. 2006, *ApJ* 648, 947
- Magorrian, J., et al. 1998, *AJ* 115, 2285
- Maoz, D., Sharon, K., Gal-Yam, A., 2010, *ApJ* in press, arXiv:1006:3576
- Mathews, W.G., 1990, *ApJ*, 354, 468
- Mathews, W.G., Baker, J.C. 1971, *ApJ* 170, 241
- Maraston, C. 2005, *MNRAS* 362, 799
- Memola, E., Trinchieri, G., Wolter, A., Focardi, P., Kelm, B., 2009, *A&A*, 497, 359
- Million, E. T., Werner, N., Simionescu, A., et al. 2010, *MNRAS* 407, 2046
- Nagino, R., Matsushita, K., 2009, *A&A*, 501, 157
- Napolitano, N. R., Romanowsky, A. J., Capaccioli, M., et al., *MNRAS*, in press (2010) (arXiv:1010.1533)
- Navarro, J. F., Frenk, C. S., White, S. D. M., 1997, *ApJ*, 490, 493
- O'Sullivan, E., Forbes D. A., Ponman T. J., 2001, *MNRAS*, 328, 461
- O'Sullivan, E., Ponman, T.J., Collins, R.S. 2003, *MNRAS* 340, 1375
- Parriott, J. R., Bregman, J. N. 2008, *ApJ* 681, 1215
- Pellegrini, S., Fabbiano, G., 1994, *ApJ*, 429, 105
- Pellegrini, S., Held, E., Ciotti, L., 1997, *MNRAS* 288, 1
- Pellegrini S., Ciotti L. 1998, *A&A* 333, 433
- Pellegrini, S., Baldi, A., Kim, D. W., Fabbiano, G., Soria, R., Siemiginowska, A., Elvis, M. 2007, *ApJ* 667, 731
- Pellegrini, S., 2010, *ApJ*, 717, 640
- Pellegrini, S., 2011, in *Hot Interstellar Matter in Elliptical Galaxies*, eds. D.W. Kim and S. Pellegrini, Astrophysics and Space Science Library, Springer (NY), in press
- Read, A.M., Ponman, T.J. 1998, *MNRAS*, 297, 143
- Revnivtsev, M., Churazov, E., Sazonov, S., Forman, W., Jones, C. 2008, *A&A* 490, 37
- Saglia, R. P., Bertin, G., Stiavelli, M. 1992, *ApJ*, 384, 433
- Sansom, A. E., O'Sullivan, E., Forbes, D.A., Proctor, R. N., Davis, D. S. 2006, *MNRAS* 370, 1541
- Sarazin, C.L., White, R.E.III, 1988, *ApJ*, 331, 102
- Sarazin, C.L., Ashe, G.A., 1989, *ApJ*, 345, 22
- Sharon, K., Gal-Yam, A., Maoz, D., et al. 2010, *ApJ*, 718, 876
- Shen, J., Gebhardt, K. 2010, *ApJ*, 711, 484
- Sun, M., Jones, C., Forman, W., Vikhlinin, A., Donahue, M., Voit, G. M., 2007, *ApJ*, 657, 197
- Tang, S., Wang, Q.D. 2005, *ApJ*, 628, 205
- Tang, S., Wang, Q.D., Mac Low, M., Joung, M.R. 2009, *MNRAS* 398, 1468
- Trinchieri, G., Pellegrini, S., Fabbiano, G., et al. 2008, *ApJ*, 688, 1000
- Weijmans, A.M., Cappellari, M., Bacon, R., et al. 2009, *MNRAS*, 398, 561
- Wernli, F., Emsellem, E., Cpoin, Y., 2002, *A&A* 396, 73
- White, R.E.III, Chevalier, R., 1983, *ApJ* 275, 69
- White, R. E.III, Sarazin, C. L., 1991, *ApJ* 367, 476

Table 1
Observed properties of the ETG sample.

Name	kT (keV)	1σ error	L_X (10^{40} erg s $^{-1}$)	σ_c (km s $^{-1}$)	Ref
(1)	(2)	(3)	(4)	(5)	(6)
NGC 720	0.54	-0.01; +0.01	5.06	241	Binney et al. 1990
NGC 821	0.15	-0.05; +0.85	2.13×10^{-3}	200	Kuntschner et al. 2010
NGC1023	0.32	-0.01; +0.02	6.25×10^{-2}	204	Kuntschner et al. 2010
NGC1052	0.34	-0.02; +0.02	4.37×10^{-1}	215	Binney et al. 1990
NGC1316	0.60	-0.01; +0.01	5.35	230	D’Onofrio et al. 1995
NGC1427	0.38	-0.11; +0.26	5.94×10^{-2}	171	D’Onofrio et al. 1995
NGC1549	0.35	-0.04; +0.04	3.08×10^{-1}	210	Longo et al. 1994
NGC2434	0.52	-0.05; +0.04	7.56×10^{-1}	205	Longo et al. 1994
NGC2768	0.34	-0.01; +0.01	1.26	205	Kuntschner et al. 2010
NGC3115	0.44	-0.10; +0.16	2.51×10^{-2}	239	Fisher 1997
NGC3377	0.22	-0.07; +0.12	1.17×10^{-2}	144	Kuntschner et al. 2010
NGC3379	0.25	-0.02; +0.03	4.69×10^{-2}	216	Kuntschner et al. 2010
NGC3384	0.25	-0.15; +0.17	3.50×10^{-2}	161	Kuntschner et al. 2010
NGC3585	0.36	-0.05; +0.06	1.47×10^{-1}	198	Fisher 1997
NGC3923	0.45	-0.01; +0.01	4.41	250	Pellegrini et al. 1997
NGC4125	0.41	-0.01; +0.01	3.18	227	Bender et al. 1994
NGC4261	0.66	-0.01; +0.01	7.02	300	Bender et al. 1994
NGC4278	0.32	-0.01; +0.01	2.63×10^{-1}	252	Kuntschner et al. 2010
NGC4365	0.44	-0.02; +0.02	5.12×10^{-1}	245	Bender et al. 1994
NGC4374	0.63	-0.01; +0.01	5.95	292	Kuntschner et al. 2010
NGC4382	0.40	-0.01; +0.01	1.19	187	Kuntschner et al. 2010
NGC4472	0.80	-0.00; +0.00	18.9	294	Bender et al. 1994
NGC4473	0.35	-0.03; +0.05	1.85×10^{-1}	192	Kuntschner et al. 2010
NGC4526	0.33	-0.01; +0.02	3.28×10^{-1}	232	Kuntschner et al. 2010
NGC4552	0.52	-0.01; +0.01	2.31	268	Kuntschner et al. 2010
NGC4621	0.27	-0.09; +0.13	6.08×10^{-2}	225	Kuntschner et al. 2010
NGC4649	0.77	-0.00; +0.00	11.7	315	Bender et al. 1994
NGC4697	0.33	-0.01; +0.01	1.91×10^{-1}	174	Binney et al. 1990
NGC5866	0.35	-0.02; +0.03	2.42×10^{-1}	159	Fisher 1997

Column (1): galaxy name. Cols. (2), (3) and (4): the hot gas temperature, its uncertainty, and the 0.3–8 keV gas luminosity, from BKF. Col. (5): the stellar velocity dispersion, as the luminosity-weighted average within an aperture of radius $R_e/8$, with its reference in Col. (6).

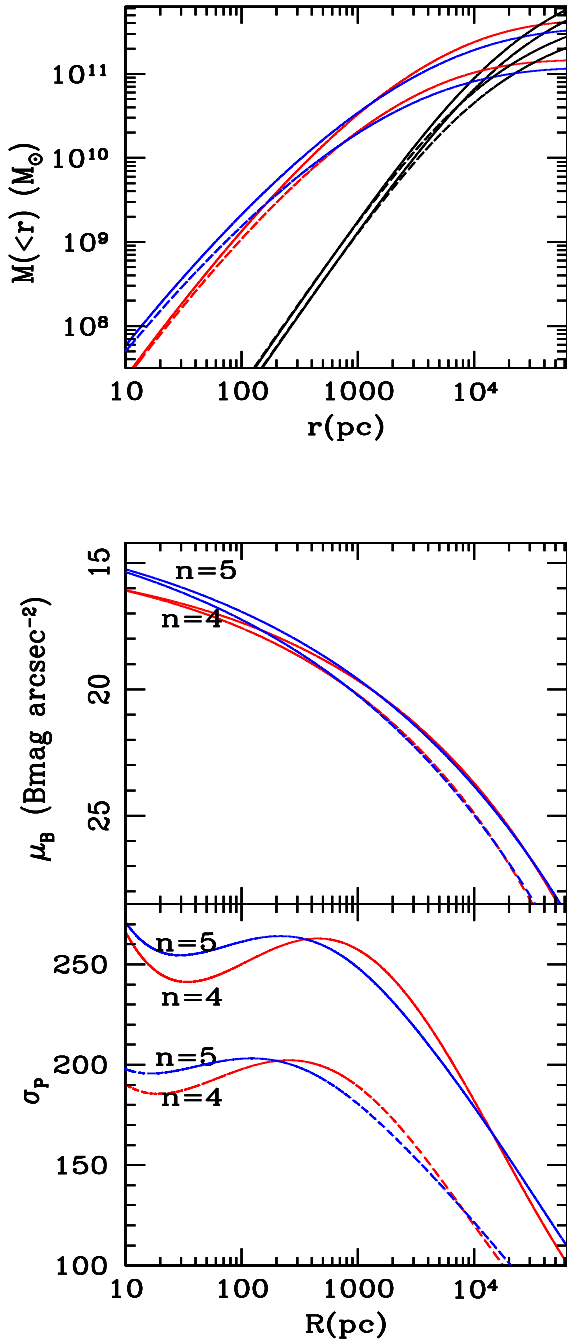


Figure 1. Mass (up), B-band surface brightness (middle), and projected velocity dispersion (bottom) profiles of three-component galaxy models (MBH+stars+dark matter), for two representative ETGs with isotropic orbits and an aperture velocity dispersion within $R_e/8$ of $\sigma_c = 260$ km s⁻¹ (solid lines; $L_B = 5 \times 10^{10} L_{B,\odot}$, and $R_e = 6.5$ kpc), and of $\sigma_c = 200$ km s⁻¹ (dashed lines; $L_B = 2 \times 10^{10} L_{B,\odot}$, and $R_e = 3.6$ kpc). Red lines refer to a stellar Sérsic profile with index $n = 4$, blue ones with $n = 5$. The dark halo in the upper panel (black, with the same line type as the corresponding stellar profile) follows the NFW profile, with $\beta = 2$, and $\mathcal{R} = 3$ (for $n = 4$) or $\mathcal{R} = 5$ (for $n = 5$), and then $\mathcal{R}_e = 0.24$ or 0.41 , from the Jeans equations (see Sect. 4).

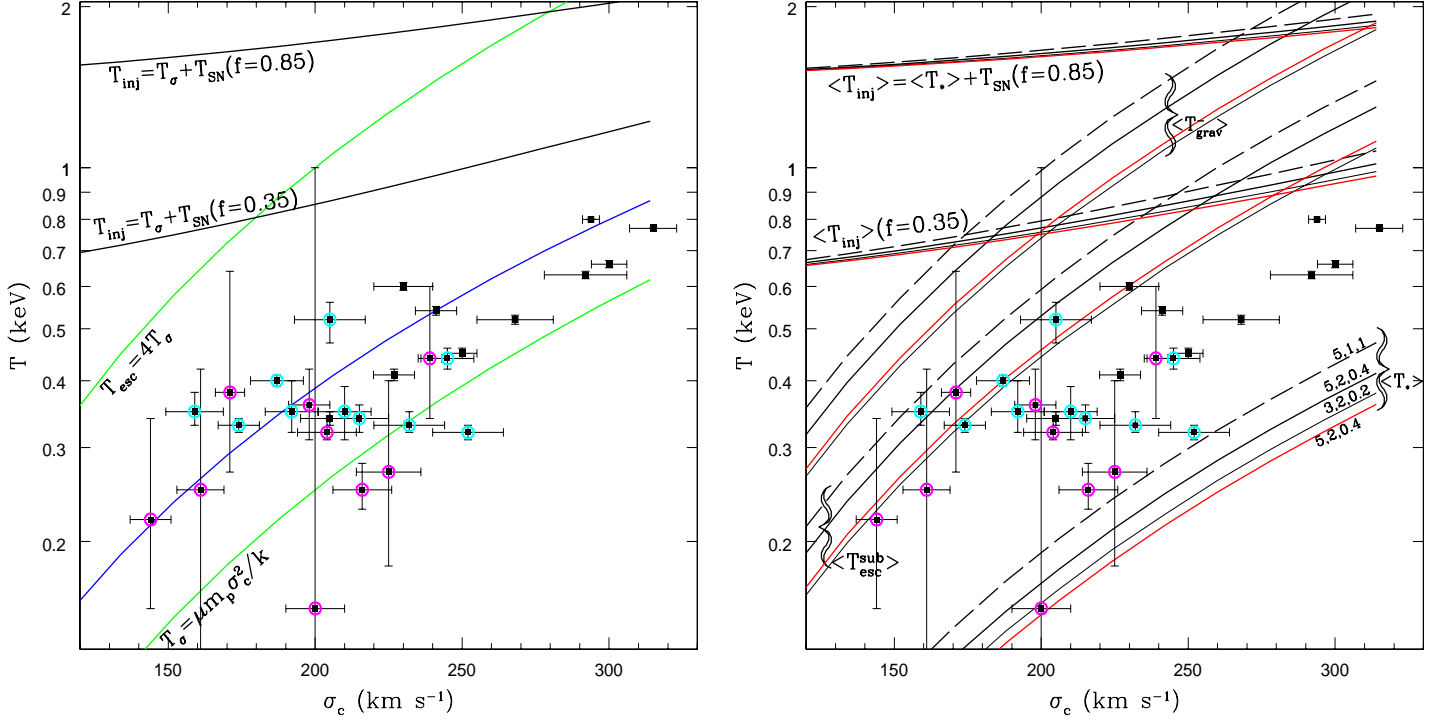


Figure 2. The relationship between the observed gas temperature (from BKF) and σ_c (see Sect. 5.1). Symbols surrounded by a magenta and cyan circle have respectively $10^{38} \text{ erg s}^{-1} < L_X < 1.5 \times 10^{39} \text{ erg s}^{-1}$, and $1.5 \times 10^{39} \text{ erg s}^{-1} < L_X < 1.2 \times 10^{40} \text{ erg s}^{-1}$; all other ETGs have larger L_X . Left panel: in green T_σ (Sect. 2), and the simple estimate of $4T_\sigma$ for the escape temperature (Sect. 3); in blue the best fit $\sigma_c \propto T^{0.56 \pm 0.09}$ found from *ROSAT* data (O’Sullivan et al. 2003); in black two cases of T_{inj} (Eq. 3), calculated using T_σ . Right panel: 1) $\langle T_* \rangle$ (Eq. 2, lowest bundle of lines), calculated for four representative galaxy mass models (made of MBH+stars+dark halo), with a Sérsic index $n = 4$ (black lines) or $n = 5$ (red line), and the dark matter parameters \mathcal{R} , β , \mathcal{R}_e indicated on each curve (Sect. 4); 2) $\langle T_{grav}^- \rangle$ and $\langle T_{esc}^{sub} \rangle$ (Sect. 3) for the same mass models adopted for $\langle T_* \rangle$, with the corresponding line type and color; 3) $\langle T_{inj} \rangle$ calculated using $\langle T_* \rangle$, with the corresponding line type and color, and $f = 0.85$ or $f = 0.35$ in Eq. 3.

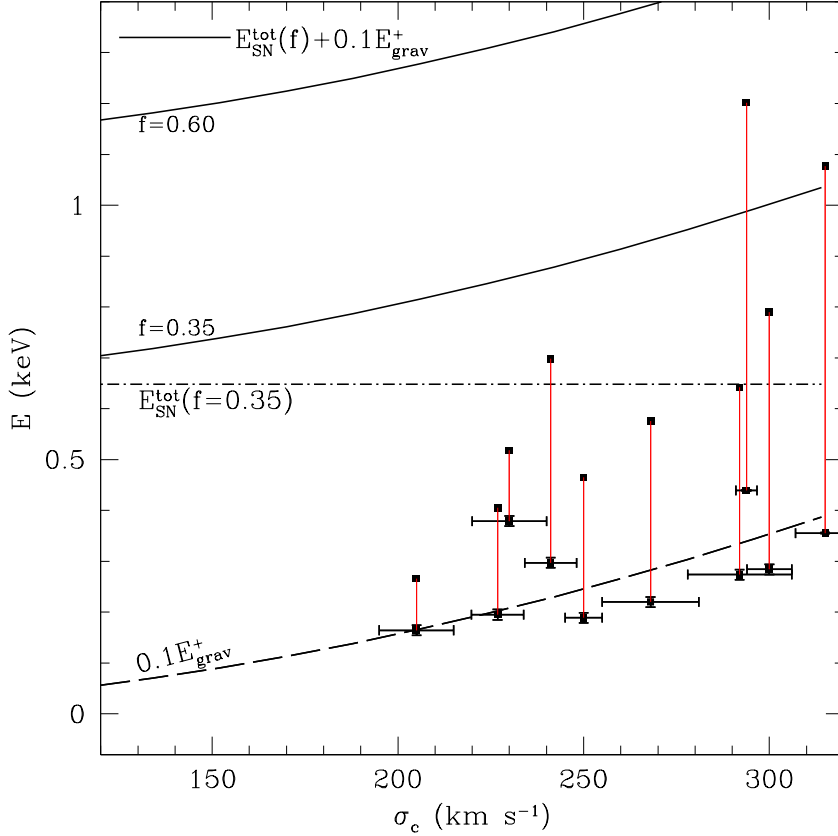


Figure 3. The run with σ_c of the energies provided by SNIa's (E_{SN}^{tot}) and gas infall (E_{grav}^+); points with errorbars show, for the ETGs with the largest L_X in Fig. 2, the additional thermal energy (ΔE_{th}) with respect to that gained from the thermalization of the stellar random motions, required to explain the observed T 's (see Sect. 5.2); all these energies (E_{SN}^{tot} , E_{grav}^+ , and ΔE_{th}), that are defined per unit mass in the text, have been multiplied by $2\mu m_p/3$ to obtain their temperature-equivalent in keV plotted here. Solid lines show the sum of the energies provided by the SNIa's and infall, for two cases of f , and for E_{grav}^+ rescaled by a factor of 0.1, and calculated for the galaxy mass model described by the thick black line in Fig. 2 (right panel). The dashed line gives for reference the value of $0.1E_{grav}^+$, and the dot-dashed line the value of E_{SN}^{tot} for $f = 0.35$. The points with errorbars are obtained subtracting to the observed kT the value of $k < T_* >$ corresponding to its σ_c , for the mass model adopted for E_{grav}^+ ; each point is linked by a red line to a point including the energy spent in radiation observed for that ETG (i.e., the upper point measures $\Delta E_{th} + L_X/\dot{M}_*$). See Sect. 5.2 for more details.

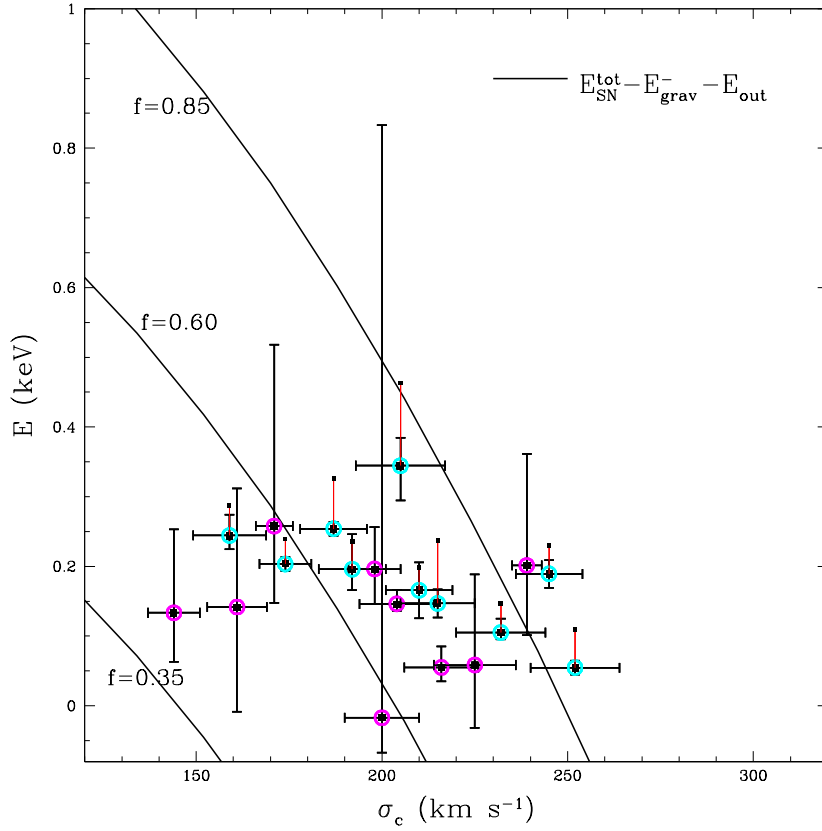


Figure 4. The run with σ_c of the energy provided by SNIa's (E_{SN}^{tot} , for three cases of f), after subtraction of the energy needed for the removal of the gas from the galaxy (E_{grav}^-), and for escape (E_{out}) at an average $v_{out} = c_s$ (0.3 keV); all energies have been computed as in Fig. 3. The adopted galaxy mass model is that corresponding to the thick black line in Fig. 2 (right panel). Points with errorbars show the additional thermal energy required to explain the observed T 's, calculated as in Fig. 3, for ETGs with low/medium L_X in Fig. 2. For the cyan ETGs, a red line connects each point with the value including the radiated energy, as in Fig. 3; the red lines of the magenta ETGs, whose L_X values are the lowest, would be included within the colored circle, if shown. See Sect. 5.3 for more details.

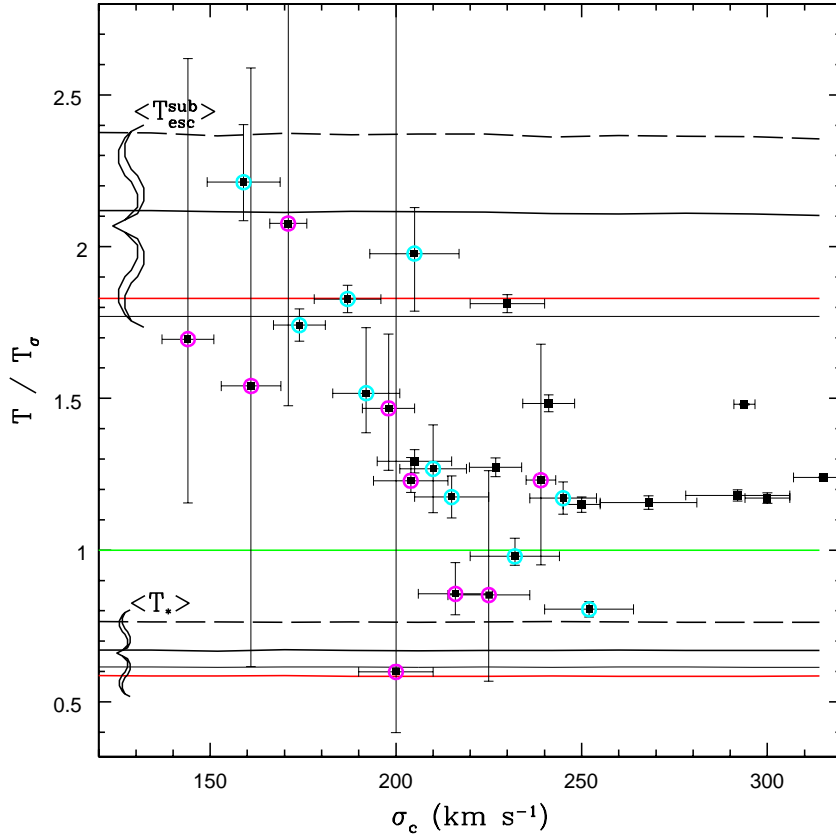


Figure 5. The same as in Fig. 2 (right panel), with temperature values rescaled by T_{σ} .